First Jicamarca radar observations of two-stream *E* region irregularities under daytime counter equatorial electrojet conditions

Ronald F. Woodman and Jorge L. Chau[1]

Radio Observatorio de Jicamarca, Instituto Geofísico del Perú, Lima, Peru

Received 6 March 2002; revised 27 August 2002; accepted 5 September 2002; published 27 December 2002.

[1] We report the first Jicamarca Radio Observatory (JRO) observations of two-stream irregularities under daytime counter equatorial electrojet (CEEJ) conditions, made with a VHF radar. This type of irregularity, although predicted by linear theory, has been observed only very few times at other sites (once in Africa and once in India). In the first 40 years of the existence of JRO, these irregularities were not observed. Since June 2000 and November 2001, we have observed them, surprisingly on seven different days. Our observations reveal that CEEJ irregularities appear only when large reversed zonal electric fields exist. We have used the horizontal component of the magnetic field due to the equatorial electrojet (ΔH) as a proxy of the zonal electric fields. Initially, the CEEJ echoes are weak, with a Doppler velocity comparable to the ion-acoustic speed, and a relatively narrow spectral width and coming only from small elevation angles. As the ΔH value gets more negative (~ -200 nT around noon), very strong CEEJ echoes appear, still with ion-acoustic velocities at low elevation angles but with large spectral widths. The Doppler shifts of the spectra follow a dependence on the cosine of elevation angle. Weak CEEJ echoes are again observed when the irregularities are about to disappear (i.e., when ΔH is just slightly negative of the threshold value). In order to get a better understanding of the scattering mechanism responsible for these echoes, we have devised a simple statistical model and compared its spectra to the spectral radar data. The CEEJ spectral characteristics can be explained on the basis of turbulent plasma breakdown of pure two-stream instabilities. These echoes are thought to be generated by nonlinear mode coupling and, when sufficiently strong, by secondary wave instabilities driven by pure two-stream waves at the density maximum and the topside of the *E* region. *INDEX TERMS:* 2439 Ionosphere: Ionospheric irregularities; 2415 Ionosphere: Equatorial ionosphere; 2471 Ionosphere: Plasma waves and instabilities; 2437 Ionosphere: Ionospheric dynamics; *KEYWORDS:* electrojet, irregularities, equatorial, Jicamarca

Citation: Woodman, R. F., and J. L. Chau, First Jicamarca radar observations of two-stream *E* region irregularities under daytime counter equatorial electrojet conditions, *J. Geophys. Res.*, *107*(A12), 1482, doi:10.1029/2002JA009362, 2002.

1. Introduction

[2] The potential of the Incoherent Scatter radar of the Jicamarca Radio Observatory (JRO) in studying the equatorial *E* region irregularities was realized at a very early stage. Recently the Observatory celebrated the 40-year anniversary of its first successful incoherent scatter observations of the ionosphere. Observations of equatorial electrojet (EEJ) irregularities at the facility have been made for a comparable period [e.g., *Bowles et al.*, 1963; *Balsley*, 1969b; *Fejer et al.*, 1975a; *Kudeki et al.*, 1987; *Hysell and Burcham*, 2000]. Despite such long history of observations JRO had not observed two-stream instabilities under daytime counter-equatorial electrojet (CEEJ) conditions as was expected by current theories and suggested by a few observations at other equatorial facilities [e.g., *Crochet et al.*, 1979; *Somayajulu et al.*, 1994]. Recently, we have now observed this phenomena, and, somewhat to our surprise, we have observed more than one event in a relatively short time.

[3] A good review of our current observational and theoretical knowledge of EEJ irregularities is given by *Farley* [1985], particularly under normal conditions, i.e., eastward (westward) electric fields during daytime (nighttime). Historically EEJ irregularities are classified into two types: type 1 due to a two-stream instability; and type 2 due to a gradient drift instability. The cause and the majority of the characteristics of both irregularity types can be explained by linear theory [e.g., *Farley*, 1985, for details].

[4] Based on linear theory, what is expected under CEEJ conditions? A daytime reversal of the EEJ (i.e., westward electric fields instead of eastward) shuts off the generation of large scale and type 2 waves, but not necessarily type 1. This

[1]Also at Laboratorio de Física, Universidad de Piura, Piura, Peru.

0148-0227/02/2002JA009362$09.00

is true if the ambient vertical density gradients remain positive ($\partial N_0/\partial z > 0$) as is the case for normal daytime conditions. Under these conditions, type 1 echoes could be generated if the reversed electric fields are large enough so that the electron drift velocity equals or exceeds the ion-acoustic velocity threshold (e.g., $C_s \sim 360$ ms^{-1}). If $\partial N_0/\partial z$ is negative, then linear theory predicts that type 2 echoes could also occur under less intense CEEJ conditions [*Farley*, 1985].

[5] For many years when daytime CEEJ conditions occurred at Jicamarca, i.e., westward electric fields, no backscatter echoes from EEJ irregularities were observed, in accordance with theory. On many occasions the incoherent scatter vertical drift velocities indicated the reverse conditions. In other days, ΔH, a measured of the horizontal magnetic field due to the EEJ current (with proper ring current subtraction), was used as a proxy measurement of the electric fields [e.g., *Rastogi*, 1974]. Typical Jicamarca observations show that type 2 irregularities get weaker as ΔH approaches zero just prior to a CEEJ event. Then, the echoes disappear completely as ΔH becomes negative but not negative enough as to generate two−stream irregularities, in agreement with linear theory. Apparently this ''threshold'' had never been surpassed, even during very disturbed conditions.

[6] The observations of CEEJ irregularities at other sites are very few. *Crochet et al.* [1979] presented the first observations of CEEJ irregularities during a very strong reversed event (ΔH ~ -60 nT). These observations were made on 21 January 1977 over Addis Ababa, Ethiopia using an HF radar. The main characteristics of those echoes were narrow spectral widths, and large Doppler velocities that depended on (a) the cosine of the radar elevation angle, and (b) the radar wavelength. *Hanuise and Crochet* [1981] attributed those echoes to a pure two-stream instability without the usual backgroundof large scale turbulence, owing to the presence of a stabilizing positive $\partial N_0/\partial z$. Later *St. Maurice et al.* [1986] attributed the behavior of these echoes to weak mode coupling.

[7] In the Indian sector, *Somayajulu and Visnawathan* [1987] reported observations of type 2 echoes during weak morning and evening CEEJ events in July 1976, using a VHF radar in Thumba, India. Later *Somayajulu et al.* [1994] reported observations of type 2 and type 1 echoes under the CEEJ event of 30 June 1987 using a VHF radar in Trivandrum, India. Type 2 spectra were observed in the presence of blanketing sporadic E (E_s) layers under a weak CEEJ, i.e., ΔH ~ -10 nT (using a nighttime base value). Type 1 spectra were observed under slightly more negative ΔH values (-35 to -40 nT) in the absence of blanketing E_s layers. The authors attributed both echoes to a destabilizing negative $\partial N_0/\partial z$. These observations have been discussed further by *Rastogi* [2001]. More recently, CEEJ irregularities have also been also observed with a VHF radar in Pohnpei (W. Ecklund, personal communication, 2001), but so far we do not have specific details of these observations.

[8] In this paper, we report the characteristics of the first CEEJ two-stream irregularities observed at Jicamarca. We first describe the main experimental setup used in our observations that yielded seven different days of two-stream CEEJ events in the last few months. Then, we present the details of our statistical scattering model and compare our simulations to the 12 August 2000 event. Finally, we discuss those comparisons and summarize our main conclusions.

2. Experimental Setup

[9] Since 1996 the JULIA (Jicamarca Unattended Long term Investigations of the Atmosphere) system has been used to observe ionospheric and atmospheric irregularities [e.g., *Hysell et al.*, 1997; *Hysell and Burcham*, 1998] almost continuously (more than 4000 hours a year). As part of these observations, EEJ irregularities have been mainly observed in the so-called oblique mode [e.g., *Balsley*, 1969b; *Fejer et al.*, 1975a; *Hysell and Burcham*, 2000], particularly during the daytime. This oblique mode points to the east and/or west of Jicamarca with small antennas to obtain information from different elevation angles. Since the EEJ irregularities are confined to a very narrow altitude region (95 and 110 km), the elevation angle information is obtained directly from range. This mode provides estimates of the electric fields and zonal winds at EEJ heights [*Balsley*, 1969a; *Balsley et al.*, 1976; *Hysell and Burcham*, 2000; *Chau et al.*, 2000; *Hysell et al.*, 2002].

[10] Between June 2000 and December 2001, we observed daytime CEEJ two-stream irregularities on seven days (8 June, 13 July, 12 August, 5 October in 2000, and 11 April, 22 October, and 6 November in 2001). These observations have been made with different antenna beams (narrow and wide to the West, wide to the East) and configurations (monostatic and interferometry), all of them under magnetically disturbed conditions. In the majority of the events, the observations were made with a COCO array pointing to the West. The beam of this array is very narrow in the North-South direction and very wide in the East-West direction, pointing $\sim$45° to the west. In addition, during the August 2000 observations, this array generated a significant pointing close to vertical (see *Hysell et al.* [2002], for more details on this configuration). This increase in the ''vertical'' sidelobe relative to a standard COCO array (-6 rather than -20 dB respect to the mainlobe) was due to a malfunction of the COCO array at the time: The gain of one of the four COCO lines was 25% weaker than the gain of the other three lines. This problem was corrected in October 2000.

[11] In this paper we will cover only the observations made on 12 August 2000 taken during magnetically disturbed condition, which present the majority of characteristics observed during the other events. Observations with the radar pointing westward were made between 85 and 240 km in range every 2 km with 30 kW of peak transmitted power. Spectral data were computed every 24 seconds with 64 points per range (R) and an interpulse period (IPP) of 2.5 ms, giving a Doppler window of ±200 Hz or ±600 ms^{-1} radial velocity.

3. Radar Observations

[12] In Figure 1 we show the range-time plots of (a) signal-to-noise ratio (SNR) and (b) Doppler velocities (positive towards the radar, i.e., to the East and downward) of the EEJ irregularities observed between 0800 and 1300 LT on 12 August 2000. The 1-minute ΔH values are denoted with a solid line in Figure 1a (see values to the right). The ΔH values were obtained by measuring the H

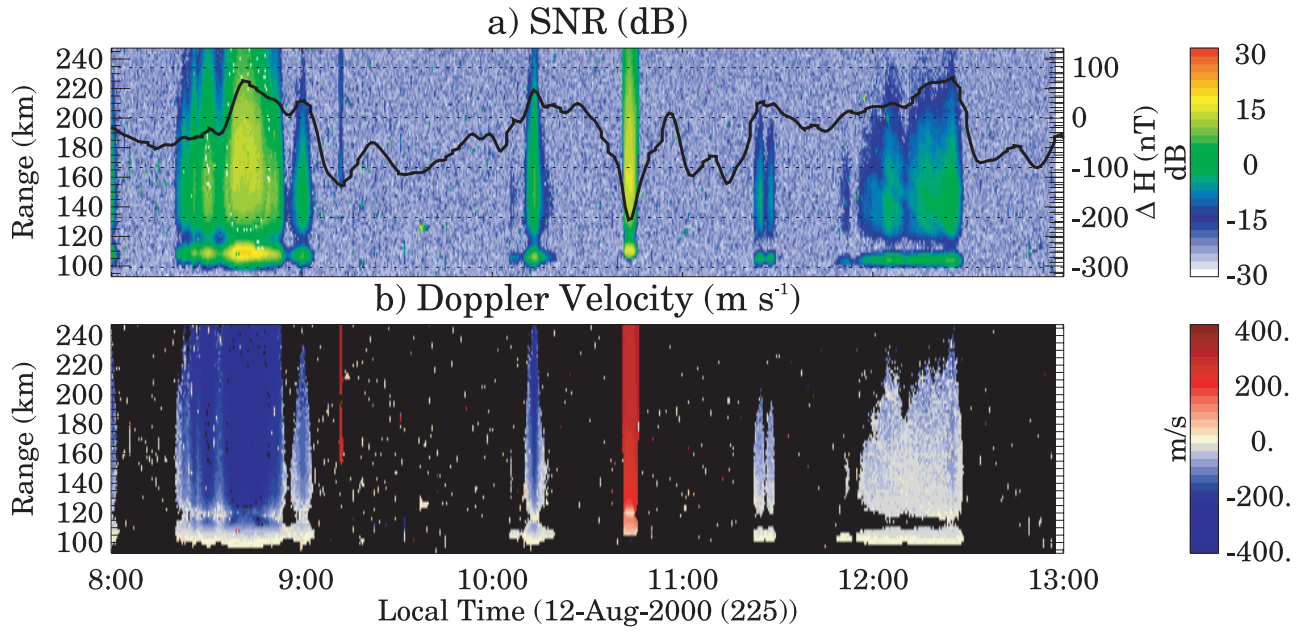

Figure 1. Range-time (a) signal-to-noise ratio (SNR), and (b) Doppler velocities, for the equatorial electrojet (EEJ) observations made on 12 August 2000. The black line in the top figure represents the 1-minute magnetometer ΔH values that correspond to the EEJ. The counter EEJ (CEEJ) events are observed around 0910 and 1045 LT and are characterized by positive Doppler velocities.

field under the EEJ region (at Jicamarca) and subtracting values measured north of the EEJ (at Fuquene, Colombia, dip latitude $\sim$16°N).

[13] We see several examples of the normal disappearance of EEJ irregularities when ΔH is moderately negative (typical behavior). However, Figure 1 also shows the reappearance of irregularities for large negative ΔH values, e.g., weakly and briefly around 0910 LT (ΔH = $-$130 nT) and more strongly at 1045 LT(ΔH = $-$200 nT). In Figure 1b, observe that the CEEJ (normal) events are accompanied by positive (negative) Doppler velocities in red (blue), i.e., eastward (westward) electron drifts.

[14] Note that the 1045 LT event occurs at a slightly higher altitude ($\sim$106 km), than the previous normal EEJ event (around 1005 LT) that occurred at $\sim$103 km. Recall, that because of the sidelobe of the COCO array, these lowest ranges correspond to vertical echoes. This slightly higher altitude is in agreement with the well known higher altitude occurrence of type 1 echoes as compared to type 2 echoes [*Fejer et al.*, 1975b; *Kudeki et al.*, 1987]. So we are pretty certain the CEEJ echoes occur under a positive or close-to-zero $\partial N_0/\partial z$.

[15] The spectrograms of the strongest CEEJ event (i.e., around 1045 LT) are presented in Figure 2. In each row, we present a spectrogram (range vs radial velocity) along with its mean power profile (in solid red) and mean spectral width (in green diamonds) on the right-hand side plot. Note that the scale of the spectral width profiles (in green) changes for each row, e.g., the first row values should be multiplied by 0.5, the second row values by 1 and so on. The inset figure on each spectrogram (labeled c in the first row, f in the second row and so on) shows a normalized spectrum (with a linear scale) at 219 km range. In addition, the estimated mean Doppler velocity obtained with via Gaussian fitting is indicated with a solid line in the spectrograms. From top to bottom we present the different stages of this event, from its initial appearance (1043 LT) until its disappearance (1048 LT).

[16] Initially the CEEJ irregularities appear stronger at larger ranges with very narrow spectral widths ($\sim$32 ms^{-1}) and high Doppler velocities ($\sim$310 ms^{-1}) (see Figures 2a, 2b and 2c). Moreover, the mean Doppler velocity shows a slight dependence on range (i.e., elevation angle),becoming smaller as the range decreases. Very similar characteristics are observed when the CEEJ irregularities are about to disappear (see Figures 2m, 2n, and 2o).

[17] When the CEEJ irregularities are fully developed (see Figures 2g, 2h and 2i), their characteristics are: (1) the mean Doppler velocity is dependent on range (or elevation angle), (2) the spectral width is larger than the initial stage and decreases with increasing range, and (3) the shape of the power as a function of range is similar to the one due to type 2 echoes observed under normal daytime EEJ conditions.

[18] Between the initial (final) and fully-developed conditions, we have shown intermediate stages of this event. See Figures 2d, 2e, and 2f (2j, 2k, and 2l) for the stage before (after) the fully-developed one. The main characteristics of these intermediate stages are: (1) the mean Doppler velocities are dependent on range, (2) the spectral widths (note that the scale changes from row to row) are larger than those from the initial stage but smaller than the fully-developed stage, and also decrease also with range, (3) the power profiles are very similar to power profiles under normal EEJ conditions.

4. A Statistical Scattering Model

[19] In order to help the reader to interpret the main scattering characteristics of the radar CEEJ echoes, in this section we present an 'ad-hoc' model of the electron density

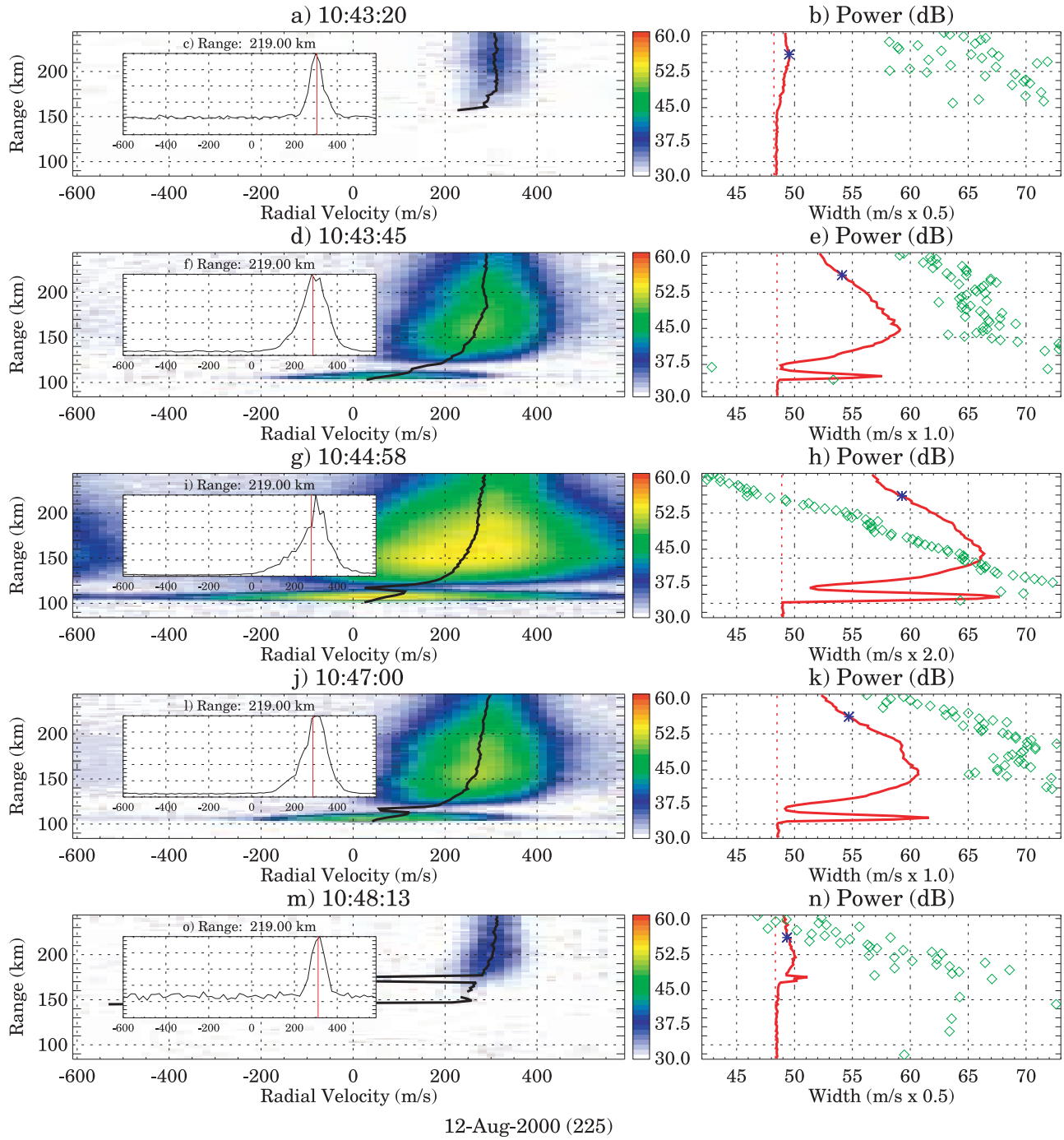

Figure 2. (a–o) CEEJ spectrograms (range vs radial velocity) and their corresponding power (in red) and spectral width (in green) profiles (right-hand plots). The estimated mean Doppler velocity is denoted with a solid black line over the spectrogram. The inset figure on each spectrogram denotes the normalized spectrum (in linear scale) at 219-km range. From top to bottom, the spectrograms are shown sequentially. Note that the scale of the spectral width changes for each row.

fluctuations that conforms with the observations. The model parameterizes the intrinsic scattering properties of the medium. The parameters include an anisotropic length scales, a mean vector velocity, and an anisotropic velocity spread. It allows us to separate automatically instrumental effects, like antenna beam pattern and other geometrical corrections, and leave only the intrinsic scattering properties of the medium (see, e.g., *Woodman* [1991] for a mathematical description of the separation of the these components). The model parameters are obtained via a cut-and-try inversion fitting procedure.

[20] We expect the model to reproduce the anisotropy of the echoes including their spectral characteristics as a function of elevation angle. The angle in this case is defined by the range of the returns, since given the stratified and narrow altitude confinement (around H_0) of the echoing

region, for a particular range, only a small angular range contributes to the echoes.

[21] The scattering properties of the medium are completely defined by their space-time electron density auto correlation function. We can build up a random density fluctuation field of electrons with any given such correlation function, and hence **k**-vector number, and frequency spectrum, by the random superposition of moving independent density blobs of electrons with deterministic electron density shape. The **k**-spectrum of the resultant fluctuations is determined by the **k**-spectrum of the blobs. The frequency spectrum is determined either by the lifetime of the blobs or by the superposition of blobs with different random velocities. In fact, both alternatives are related, and there are different ways of explaining a given velocity spectral width. We have chosen the second alternative for our model. The mean Doppler shift is defined by the mean velocity of the blobs.

[22] The narrow altitude confinement of the echoing region is easily modeled by confining the existence of the blobs to the observed altitude range of the echoes. Although it is possible to reproduce a smooth altitude profile, we have used a simple uniform, but confined, region of fluctuations with a comparable width to the one observed ($H_0 \pm 2.0$ km).

[23] The radar backscattering technique provides information about only a very limited region in **k**-space, namely a narrow annular region of radius k_B, where k_B is the Bragg scattering wavelength, 3 meters in our case, equal to half the radar wavelength. Therefore, we have plenty of freedom to chose the shape of the blob. The only constraint is that it should satisfy the observed characteristics in this narrow region of the whole **k** space. We have used a Gaussian shape and characteristic size (σ_x) for analytical convenience. We have used blobs with dimensions comparable to $\mathbf{k}_B^{-1}$ and adjust it shape to be anisotropic in the vertical EW plane with different dimensions for its vertical (σ_z) and zonal ($\sigma_x \sim 1/k_B$) widths. The degree of anisotropy is adjusted to conform with the observations. Furthermore, we have used infinitely elongated blobs (tubes) along the North-South, i.e., the y direction parallel to **B**.

[24] From observations the spectral shape in the frequency domain are bell-shaped. Again, for convenience, we have used Gaussian shapes. Furthermore, since any scattering region is subjected to the random superposition of driving forces, we could argue that a Gaussian shape is good on theoretical grounds, based on the central limit theorem. We therefore allowed our blobs to have a random velocity following a Gaussian probability distribution function, with a mean velocity vector ($\bar{v}_x$, $\bar{v}_z$),and zonal and vertical variances (σ_u^2 and σ_w^2, respectively) that we adjust to fit our observations. A Gaussian velocity distribution function results, as we see below, in a Gaussian shaped frequency spectrum. We have allowed the velocity distribution function to be anisotropic (i.e., $\sigma_x \neq \sigma_z$) which is necessary for our model to fit the observations.

[25] According to the above discussion, we are analytically modeling our elementary blobs with an electron density η, at position **x** and time t, given by

$$\eta[\mathbf{x}, t; \mathbf{v}] = \frac{\exp\left(-\frac{(-v_x t - x_{ox} + x_x)^2}{2\sigma_x^2} - \frac{(-v_z t - x_{oz} + x_z)^2}{2\sigma_z^2}\right)}{2\pi\sigma_x\sigma_z} \tag{1}$$

[26] Given the statistical independence of the different blobs, the space-time auto correlation function of N blobs ($\rho[\mathbf{r},\tau]$), is equal to N times the autocorrelation function of a single blob, i.e.,

$$\rho[\mathbf{r}, \tau] = N < \eta[\mathbf{x}, t; \mathbf{v}]\eta[\mathbf{x} + \mathbf{r}, t + \tau; \mathbf{v}] > \tag{2}$$

[27] We can evaluate the average through the expectation of the expression in the brackets using the probability distribution functions of the random parameters $\mathbf{x}_o$ and velocity **v**. We use an even distribution in space and an anisotropic Gaussian distribution in velocity as mentioned above. Such a choice conforms very well with the spectral observations. Once the average is performed, we obtain a space-time autocorrelation of the medium

$$\rho[\mathbf{r}, \tau] = \frac{\exp\left(-\frac{(r_x + \bar{v}_x\tau)^2}{4\sigma_x^2 + 2\sigma_u^2\tau^2} - \frac{(r_z + \bar{v}_z\tau)^2}{4\sigma_z^2 + 2\sigma_w^2\tau^2}\right)}{2\pi\sqrt{\left(2\sigma_x^2 + \sigma_u^2\tau^2\right)\left(2\sigma_z^2 + \sigma_w^2\tau^2\right)}} \tag{3}$$

[28] The radar actually measures the space-time Fourier transform of ρ, $F[\mathbf{k},w]$, evaluated at the particular $\mathbf{k} = (k_x,k_z)$ corresponding to a vector with magnitude k_B, and direction given by the line of sight, with zenith angle given by $\theta = \arccos[h/R]$, where h and R are height and range respectively. If we perform this transformation, we obtain an expression for $F[\mathbf{k},\omega]$ given by

$$F[\mathbf{k}, \omega] = \frac{\exp\left(-\frac{(k_x\bar{v}_x + k_z\bar{v}_z - \omega)^2}{2\left(k_x^2\sigma_u^2 + k_z^2\sigma_w^2\right)} - k_x^2\sigma_x^2 - k_z^2\sigma_z^2\right)}{2\pi\sqrt{k_x^2\sigma_u^2 + k_z^2\sigma_w^2}} \tag{4}$$

The vector (k_x, k_z) is given by ($k_B \sin\theta$, $k_B \cos\theta$) related to the zenith angle and the range. We can therefore express the intrinsic differential cross-section as a function of frequency and range.

[29] The observed frequency spectrum of the backscatter signals involves further integrations considering that the echo for a particular range comes from a range of angles as a consequence of the finite width of the echoing layer. This further integration, weighted by the gain of the actual antenna pattern, has been performed numerically. The frequency is directly related to velocity as a Doppler shift ($v_r = \lambda\omega/4\pi$), as we have done it in the presentation of the experimental results. We have also performed this change of variable, so that we can compare the model with the actual response in comparable terms.

[30] As a consequence of the angular integration which adds the contributions of all active angles to a given range, it is interesting to note that for ranges comparable to the altitude of the electrojet, the angles involved cover a relatively large region around zenith. The integration then includes a larger volume as compared with ranges that are much greater than the electrojet altitude. The consequence of this is that the echoes coming from ranges comparable to the altitude of the electrojet are enhanced, due to the greater contributing scattering volume, than those corresponding to higher ranges. For the particular August 2000 observations, this enhancement is exaggerated by the unusual magnitude

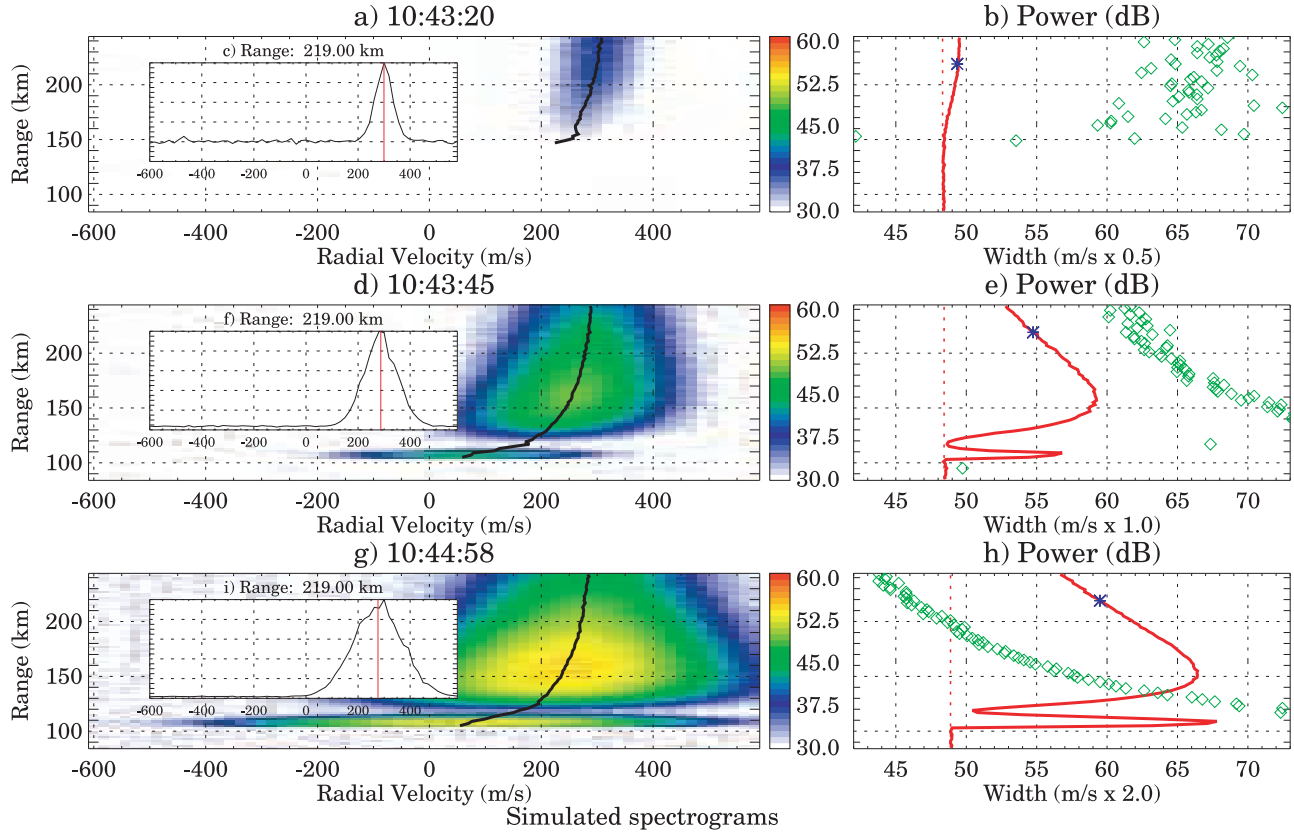

Figure 3. (a–i) Simulated CEEJ spectrograms. The three rows corresponds to the first three rows of Figure 2, respectively. The information shown is similar to the one presented for the radar results.

of the antenna vertical sidelobe. In fact, the model helped us to discover the antenna problem.

[31] It should be stressed that the model for the statistical properties of the medium is an statistical construct. It is not a model of the physical processes involved. It is always possible to build a random process with a given space-time autocorrelation function, with a properly randomized superposition of deterministic blobs of proper shape. On the other hand, the parameters chosen to best fit the data, do have physical implications. It is the case, for instance, that a single almost horizontal mean velocity, comparable to the two-stream velocity, fits the data well (as we see below), with important physical implications. Most importantly, allow us to separate instrumental effects like the one associated with the antenna pattern discussed above.

[32] In Figure 3, we present three simulated spectra as a function of radial velocity and range for different conditions corresponding to the experimental results presented in the first three rows of Figure 2. Recall that in Figure 2, the experimental results of the first (second) row, i.e., the appearance (intermediate) stage, are very similar to the results of the last (fourth) row, i.e., the disappearance (intermediate) stage.

[33] The available parameters in the model have been adjusted to obtain a good agreement via a cut and try approach. Namely, we have modified the model parameters manually to fit just two radar spectra: one from the lowest elevation angle (largest range), and one from zenith. The model spectra at other angles (ranges) were infer from the fitted parameters. The corresponding model parameters adjusted (i.e., $\bar{v}_x$, $\bar{v}_z$, σ_u, σ_w, σ_z/σ_x, and H_0) are presented in Table 1. Note that in all cases the horizontal drift velocity is comparable to C_s.

[34] We should recall that only the mean Doppler frequency and Doppler spread is due to the intrinsic properties of the medium. The mean power is mainly a consequence of the antenna pattern and the size of the scattering volume defined by the range, pulse length, the electrojet depth and the geometry that corresponds to each range gate, all of them known parameters and easy to include in the model. Nevertheless, a proper value for the anisotropy (i.e., $\sigma_x \neq \sigma_z$), another intrinsic property of the medium, is also needed to match the power vs. range observations.

5. Discussion

[35] It is evident that our model fits the results very well and, therefore, our radar observations could be summarized

Table 1. Model Parameters for the CEEJ Events Observed Over Jicamarca on 12 August 2000

Event	$\bar{v}_x^a$	$\bar{v}_z^a$	σ_u^a	σ_w^a	$(\sigma_z/\sigma_x)^b$	H_0 (km)
10:43:20	340	0	35	35	4.5	104
10:43:45	302	42	55	90	1.8	106
10:44:58	295	43	63	159	1	107

[a]In ms^{-1}.
[b]Where $\sigma_x = 1/k_B$.

by the model parameters presented in Table 1. But what are the physical causes of the different scattering characteristics? We divide our discussion mainly in two cases: (1) weak CEEJ echoes at the beginning and at the end of an event, and (2) strong CEEJ echoes with radial velocities comparable to C_s at low elevation angles in between.

[36] We have modeled the first case (i.e., the weak-CEEJ echoes) with highly anisotropic blobs, moving on the average with horizontal velocities comparable to the required threshold to excite two-stream instabilities. If we Fourier transform the density blobs and filter out only those components with wave number vectors equal to the Bragg wavelength, we are left with a quasi sinusoidal field with planar North-South vertical wave fronts and with little structure in the vertical (consequence of the high anisotropy selected). We conclude then that at the onset of the irregularities, when two-stream conditions are just met, and the **k**-vector of the instabilities are primarily horizontal. We recall the observational fact that no type II instabilities exist before then, due to the positive or close-to-zero $\partial N_0/\partial z$. This is the closest to pure two-stream linear instability conditions that we can imagine, with little nonlinear coupling. Similar conditions exist at the end of the event, shortly before the threshold condition ceases to exist.

[37] Our weak CEEJ observations, i.e., at the beginning and at the end of the CEEJ event including also what we have called the intermediate stages (see the second and fourth rows in Figure 2), are very similar to the CEEJ observations reported by *Crochet et al.* [1979], i.e., mean Doppler shifts dependent on the cosine of elevation angle, and narrow spectral widths. *Hanuise and Crochet* [1981] called them "type 0" echoes and attributed them also to pure two-stream waves under a positive stabilizing density gradient. As in our intermediate stages, the level of turbulence they found was weaker than normal daytime conditions, i.e., eastward electric fields (see Table 1). Later *St. Maurice et al.* [1986] attributed the type-0 behavior to weak mode coupling also under stabilizing conditions to explain the slightly larger spectral widths (as compared to normal type-1 spectra) but still small compared to normal conditions.

[38] For the second case (i.e., the strong-CEEJ echoes), we increase the level of the fluctuations (about 16 dB) to match the increased power observed and remove the highly anisotropic conditions. The scattering process is now isotropic, i.e., $\sigma_z = \sigma_x$, the Doppler velocities are dependent on the cosine of the elevation angle, and in both zonal and vertical directions the velocity spread is wider corresponding to a turbulent medium.

[39] *Kudeki et al.* [1987] observed a similar instability situation during a strong normal EEJ at the topside of the *E* region where drifts velocities were comparable to C_s under stabilizing conditions (negative density gradient). Since then, this type of irregularity has been called topside pure two stream. Although they observed the echoes only with a vertical pointing antenna, their interpretation could explain also our strong CEEJ echoes. Namely, *Kudeki et al.* [1987] postulated that the vertical 3-meter waves result from the nonlinear interaction of two (two-stream unstable) almost horizontal smaller wavelengths that were excited first as suggested by linear theory under a stabilizing $\partial N_0/\partial z$. Oblique waves could be also generated following similar arguments and explaining the cosine dependence of the Doppler velocities for which we provide evidence.

[40] When the strong-CEEJ echoes are observed, they are as strong as the ones obtained during normal daytime two-stream conditions. This assertion is based on a qualitative comparison with normal EEJ data obtained under similar (but reversed electric field) conditions, including the same modified antenna, same time of the day and similar magnitude of the ΔH component. So we need an equally efficient mechanism. We would like to propose a secondary instability process where horizontal gradients of longer and strong two-stream waves generate gradient-drift unstable waves in the vertical direction. These secondary waves destroy the nice coherence phase front of the initial 3-meter horizontal waves, and in its extreme, generate isotropic fluctuations at this length scale. This structure would move horizontally with the drift velocity of the electrons, riding on the phase fronts of the longer wavelengths in a way similar to white-caps in ocean waves. Then, they would produce Doppler velocities with a cosine dependence as observed. Furthermore, the (vertical) secondary instabilities will broaden the vertical spectrum more efficiently than the horizontal spectrum, as it is actually observed.

[41] Plasma fluctuations in a turbulent state are difficult to discuss analytically. The feasibility of the mechanism proposed would best be checked by numerical simulations [e.g., *Oppenheim et al*,. 1996]. We hope our observations will motivate modelers to run their numerical codes under these conditions. Needless to say the situation could not be simpler since there is no background density gradient involved. They correspond to a boundless homogeneous conditions at least for wavelengths shorter than the characteristic width of the electrojet.

[42] In any case, we can argue in favor of this mechanism (horizontal gradients of longer waves generating gradient-drift unstable waves in the vertical direction), by noting that under no-gradient conditions, large and small scale waves reach the unstable threshold for the same electron drift velocities [see, e.g., *Hanuise and Crochet*, 1981, Figure 1]. In fact, longer (than 3 meters) wavelengths have been observed [*Crochet et al.*, 1979]. Also *Farley* [1963] in his kinetic approach show that for marginal conditions, i.e., drift velocities barely above the threshold, longer wavelengths have shorter growth times. The secondary instabilities will be helped by the seeding of waves produced by nonlinear coupling, which of course, will always be there.

[43] One of the reviewers has argued against the possibility of secondary instabilities on a long primary two-stream wave because of the 90° phase relationship between the primary density gradients and the induced transverse drift velocity. Indeed 90° is not optimum, but still would produce almost half of the volume to be unstable, albeit with gradients and drifts only half as large as the maximum amplitudes occurring elsewhere. Nevertheless, these are regions that are unstable. If the unstable primary waves exist, as we postulate, they will grow until a limiting breakdown occurs. These regions of dissipation could be confined to a fraction of the total volume they occupy. The ocean white-caps are an example of a similar mechanism.

[44] The spectral widths of the data can be interpreted as a consequence of the finite coherence lifetime of 3-meter

components responsible of the scattering. This lifetime can be due to the self interference of different 3-meter waves moving with slightly different velocities, $\bar{v}_x \pm \sigma_u$ and $\bar{v}_z \pm \sigma_w$ in our model, all within the scattering volume (or statistically similar, but smaller subvolumes). This dispersion of velocities is easy to accept in a turbulent-like field. It is intuitively expected that this dispersion should be larger as the irregularities and the turbulence associated with them become larger or stronger. Indeed, the observations require larger values for σ_u and σ_w as they evolve into more developed conditions.

[45] From the observational point of view, we suggest the use of shorter and longer radar wavelengths with oblique beams in future experiments. It would also be interesting to observe the topside pure two-stream waves at different elevation angles, since these echoes could be observed more frequently. Unfortunately it is difficult to observe just the topside with oblique antennas since at given range the scattering volume involves normally the whole EEJ region, i.e., both the stable and the unstable sides. We plan to study the angular behaviour of the topside echoes using sufficiently narrow oblique beams to discriminate the bottom from the top of the EEJ region.

[46] Finally, from a linear two-stream instability point of view, we should expect only a horizontal mean velocity, $\bar{v}_x$, for the primary waves. We have found the need to include a relatively large mean vertical component, $\bar{v}_z$, to fit the spectra of the vertical components. At this point, we do not have a suitable explanation for this vertical velocity. It is also surprising that the horizontal velocity decreases slightly while the vertical velocity increases when ΔH gets more negative (see Table 1). One possibility is that, the velocity spread favors velocities lower than the two-stream velocity threshold, causing a slight skewness in the spectra.

6. Conclusions

[47] We have observed, for the first time in nearly 40 years of Jicamarca operations, two-stream radar echoes from *E* region irregularities during daytime CEEJ conditions. The observations conform well with our expectations based on existing linear theories for stable vertical density gradients, particularly when the echoes appear or are about to disappear (weak CEEJ conditions). They appear suddenly when the drift velocity approaches two-stream threshold conditions. As the electron flow increases, the mean Doppler shift shows a cosine dependence as a function of the elevation angle and larger spectral widths. These features could be due to a nonlinear mode coupling process like the one that explains the pure two-stream irregularities observed under strong normal conditions at the topside of the EEJ region. We further postulate a turbulent break down of longer two-steam unstable horizontal waves into secondary gradient drift instabilities which include the close-to-vertical 3-m waves we observed. But numerical simulations are needed to reproduce and understand the very turbulent echoes that occur after the CEEJ pure two-stream echoes. The reported increase in frequency of observations is due mainly to the large increase in observation time using the JULIA radar system and possibly coincides with the maximum of magnetic activity within the 11-year solar cycle.

[48] **Acknowledgments.** We thank J. Arias (Instituto Geográfico Agustín Codazzi, Colombia) and O. Veliz (Radio Observatorio de Jicamarca) for providing the magnetometer information. We also thank Don Farley, Mike Kelley, Erhan Kudeki, and Wes Swartz for their comments and suggestions during the early stages of the manuscript. The Jicamarca Radio Observatory is operated by the Instituto Geofísico del Perú, with support from the NSF Cooperative Agreements ATM-9408441 and ATM-9911209. Arthur Richmond thanks Christian Hanuise, David Hysell, and Erhan Kudeki for their assistance in evaluating this paper.

References

Balsley, B. B., Measurement of electron drift velocities in the night-time equatorial electrojet, *J. Atmos. Sol. Terr. Phys.*, *31*, 475–478, 1969a.

Balsley, B. B., Some characteristics of non-two-stream irregularities in the equatorial electrojet, *J. Geophys. Res.*, *74*, 2333–2347, 1969b.

Balsley, B. B., B. G. Fejer, and D. T. Farley, Radar measurements of neutral winds and temperatures in the equatorial E region, *J. Geophys. Res.*, *81*, 1457–1459, 1976.

Bowles, K. L., B. B. Balsley, and R. Cohen, Field aligned *E*-region irregularities identified with acoustic plasma waves, *J. Geophys. Res.*, *68*, 2485–2501, 1963.

Chau, J. L., D. T. Farley, and B. B. Balsley, East-west asymmetry in type 1 electrojet echoes at Jicamarca, paper presented at X International Symposium on Equatorial Aeronomy, Antalya, Turkey, 17–23 May 2000.

Crochet, M., C. Hanuise, and P. Broche, HF radar studies of two-stream instability during an equatorial counter-electrojet, *J. Geophys. Res.*, *84*, 5223–5233, 1979.

Farley, D. T., A plasma instability resulting in field-aligned irregularities in the ionosphere, *J. Geophys. Res.*, *68*, 6083–6097, 1963.

Farley, D. T., Theory of equatorial electrojet plasma waves: New developments and current status, *J. Atmos. Sol. Terr. Phys.*, *47*, 729–744, 1985.

Fejer, B. G., D. T. Farley, B. B. Balsley, and R. F. Woodman, Oblique VHF radar spectral studies of the equatorial electrojet, *J. Geophys. Res.*, *80*, 1307–1312, 1975a.

Fejer, B. G., D. T. Farley, B. B. Balsley, and R. F. Woodman, Vertical structure of the VHF backscattering region in the equatorial electrojet and the gradient drift instability, *J. Geophys. Res.*, *80*, 1313–1324, 1975b.

Hanuise, C., and M. Crochet, 5- to 50-m wavelength plasma instabilities in the equatorial electrojet, 3, Counter-electrojet conditions, *J. Geophys. Res.*, *86*, 7761–7766, 1981.

Hysell, D. L., and J. D. Burcham, JULIA radar studies of equatorial spread *f*, *J. Geophys. Res.*, *103*, 29,155–29,167, 1998.

Hysell, D. L., and J. D. Burcham, Ionospheric electric field estimates from radar observations of the equatorial electrojet, *J. Geophys. Res.*, *105*, 2443–2460, 2000.

Hysell, D. L., M. F. Larsen, and R. F. Woodman, JULIA radar studies of electric fields in the equatorial electrojet, *Geophys. Res. Lett.*, *24*, 1687–1690, 1997.

Hysell, D. L., J. L. Chau, and C. G. Fesen, Effects of large horizontal winds on the equatorial electrojet, *J. Geophys. Res.*, *107*(A8), 1214, doi:10.1029/2001JA000217, 2002.

Kudeki, E., B. G. Fejer, D. T. Farley, and C. Hanuise, The Condor equatorial electrojet campaign: Radar results, *J. Geophys. Res.*, *92*, 13,561–13,577, 1987.

Oppenheim, M., N. Otani, and C. Ronchi, Saturation of Farley-Buneman instabilities in the ionosphere, *J. Geophys. Res.*, *101*, 17,273–17,286, 1996.

Rastogi, R. G., Westward equatorial electrojet during daytime hours, *J. Geophys. Res.*, *79*, 1503–1512, 1974.

Rastogi, R. G., Ionospheric *E*-region irregularities during equatorial counter electrojet, *Indian J. Radio Space*, 130–137, 2001.

Somayajulu, V. V., and K. S. Visnawathan, VHF radar observations during equatorial counter electrojet events, *Indian J. Radio Space Phys.*, *16*, 380–383, 1987.

Somayajulu, V., R. Selvamurugan, C. V. Devasia, and L. Cherian, VHF backscatter observations of type I waves during a counter electrojet event, *Geophys. Res. Lett.*, *21*, 2047–2050, 1994.

St. Maurice, J. P., C. Hanuise, and E. Kudeki, On the dependence of the phase velocity of equatorial irregularities on the polarization electric filed and theoretical implications, *J. Geophys. Res.*, *91*, 13,493–13,505, 1986.

Woodman, R. F., A general statistical instrument theory of atmospheric and ionospheric radars, *J. Geophys. Res.*, *96*, 7911–7928, 1991.

J. L. Chau and R. F. Woodman, Radio Observatorio de Jicamarca, Apartado 13-0207, Lima, Peru. (chau@geo.igp.gob.pe; ronw@geo.igp.gob.pe)